Helsinki University of Technology, Institute of Mathematics, Research Reports
Teknillisen korkeakoulun matematiikan laitoksen tutkimusraporttisarja
Espoo 2006 A498

GOAL-ORIENTED ERROR ESTIMATES BASED ON DIFFERENT FE-SPACES FOR THE PRIMAL AND THE DUAL PROBLEM WITH APPLICATIONS TO FRACTURE MECHANICS

Marcus Rüter Sergey Korotov Christian Steenbock

TEKNILLINEN KORKEAKOULU
TEKNISKA HÖGSKOLAN
HELSINKI UNIVERSITY OF TECHNOLOGY
TECHNISCHE UNIVERSITÄT HELSINKI
UNIVERSITE DE TECHNOLOGIE D'HELSINKI

Helsinki University of Technology, Institute of Mathematics, Research Reports
Teknillisen korkeakoulun matematiikan laitoksen tutkimusraporttisarja
Espoo 2006 A498

GOAL-ORIENTED ERROR ESTIMATES BASED ON DIFFERENT FE-SPACES FOR THE PRIMAL AND THE DUAL PROBLEM WITH APPLICATIONS TO FRACTURE MECHANICS

Marcus Rüter **Sergey Korotov** **Christian Steenbock**

Helsinki University of Technology
Department of Engineering Physics and Mathematics
Institute of Mathematics

Marcus Rüter, Sergey Korotov, Christian Steenbock: *Goal-oriented Error Estimates based on Different FE-Spaces for the Primal and the Dual Problem with Applications to Fracture Mechanics*; Helsinki University of Technology, Institute of Mathematics, Research Reports A498 (2006).

Abstract: *The objective of this paper is to derive goal-oriented a posteriori error estimators for the error obtained while approximately evaluating the nonlinear J-integral as a fracture criterion in linear elastic fracture mechanics (LEFM) using the finite element method. Such error estimators are based on the well-established technique of solving an auxiliary dual problem. In a straightforward fashion, the solution to the discretized dual problem is sought in the same FE-space as the solution to the original (primal) problem, i.e. on the same mesh, although it merely acts as a weight of the discretization error only. In this paper, we follow the strategy recently proposed by Korotov et al. [13, 12] and derive goal-oriented error estimators of the averaging type, where the discrete dual solution is computed on a different mesh than the primal solution. On doing so, the FE-solutions to the primal and the dual problems need to be transferred from one mesh to the other. The necessary algorithms are briefly explained and finally some illustrative numerical examples are presented.*

AMS subject classifications: 65N15, 65N30, 65N50, 74R10

Keywords: A posteriori error estimation, finite elements, fracture mechanics

Correspondence

Marcus.Ruter@hut.fi, skorotov@hut.fi, csteenbock@gmx.com

ISBN 951-22-8129-5
ISSN 0784-3143

Helsinki University of Technology
Department of Engineering Physics and Mathematics
Institute of Mathematics
P.O. Box 1100, 02015 HUT, Finland
email:math@hut.fi http://www.math.hut.fi/

1 Introduction

In fracture mechanics, an engineer is mainly interested in whether a pre-existing macroscopic crack starts to propagate or not. In practice it means that a suitable fracture criterion has to be computed, which provides the required information. In general, such a fracture criterion is a vector-valued quantity, since also the direction of the propagating crack has to be taken into account. One such criterion is the material force acting on the crack tip. In this paper, however, we confine ourselves to symmetric problems in terms of geometry and boundary conditions as well as to isotropic elastic structures. In this case, the crack direction is clearly known a priori and thus only the material force projected into the direction of crack propagation is of importance. This (scalar-valued) fracture criterion is well known as the J-integral, originally due to Cherepanov [6] and Rice [15]. Generally, the J-integral can only be computed numerically, e.g. with the finite element method. Thus, for reliable predictions of crack propagation it is clearly of the utmost importance to control the resulting error of the J-integral.

This type of error control leads to the approach of goal-oriented adaptive finite element methods, as introduced by Eriksson et al. [8] and developed further by Becker and Rannacher [4] and others. In recent years, goal-oriented error estimates have also been developed and succesfully applied to the field of fracture mechanics, see Rüter et al. [17, 24, 20, 21], Giner et al. [9], Heintz et al. [10] and Xuan et al. [27]. Remarkably, the first steps in this direction had already been taken in 1984 by Babuška and Miller [3].

Goal-oriented error estimates are based on the solution of an auxiliary dual problem. In computational practice, the dual problem is generally solved by the finite element method. More precisely, it is conventional practice to solve it on the same finite element mesh as the primal problem. From an implementational point of view, this proves convenient, since—for linear problems—only the right-hand side has to be replaced for the dual problem once the primal problem is solved.

One has to take into account, however, that apart from the primal problem, the dual problem and the error estimator itself, which usually also requires some postprocessing in terms of auxiliary problems at the element level, have to be computed in each adaptive step. Since the dual problem is only solved in order to estimate the error, the computational costs for the total error estimation procedure are therefore higher than solving the primal problem, at least in the linear case.

Recently, Korotov at al. [13, 12] proposed a new strategy that reduces the computational costs for the error estimator in each adaptive step considerably and, at the same time, generalizes the canonical approach of solving the primal and the dual problem on the same finite element mesh. In their strategy, the dual problem is solved on an arbitrary mesh which can, as a special case, be the same as the mesh associated with the primal problem. In this fashion, it becomes possible to solve the dual problem on a coarser mesh than the primal problem which does not necessarily have to be carried

out in each adaptive step. Furthermore, it becomes possible to solve the dual problem only once on a very fine mesh, the computation of which is clearly more expensive than on a coarser mesh but has to be carried out only once for the entire adaptive mesh refinement scheme. This proves especially convenient in terms of computational costs if one is to estimate the error for the case of different boundary conditions for the primal problem which is a usual case in engineering practice when, e.g., different load cases have to be investigated. In this case, the conventional way of solving the dual problem on the same mesh in each adaptive step requires the solution of n times more global dual problems where n is the number of load cases times the number of adaptive mesh refinement steps in each load case.

It should be clear that in this strategy, additional computational challenges arise, since the solutions of the primal and the dual problem have to be transferred from one mesh to the other. Particularly, when applied to problems in fracture mechanics, even the dual load depends on the solution of the primal problem which therefore has to be transferred onto the dual mesh. Moreover, for the error estimator proposed in this paper an additional term has to be computed compared to the conventional way of using the same finite element mesh for the primal and the dual problem. This term, however, is always exactly computable in the sense that all quantities are known from the finite element computation. Summarizing these additional costs, it should nevertheless be clear that they are not as expensive as solving an additional global problem in each adaptive step.

In this paper, the strategy described above is applied to problems in LEFM as a novel approach to estimate the error of the fracture criterion. More precisely, we extend the strategy proposed by Korotov at al. [13, 12] to the case of nonlinear goal quantities of interest as elaborated in Rüter and Stein [21], where, however, the error estimators presented rely on the same mesh for both the primal and the dual problem.

The paper is organized as follows: In Section 2, the boundary value problem of linearized elasticity is introduced and the J-integral as a fracture criterion is presented. Subsequently, in Section 3 we discuss the construction of the dual data as required in order to solve the dual problem. Furthermore, we derive the error representation for the error of the J-integral that is based on the solution of the dual problem. In Section 4, we focus on averaging-based error estimation techniques for the error of the J-integral based on the dual solution. Finally, two illustrative numerical examples are presented in Section 5 before the paper concludes with Section 6, which summarizes the major findings achieved from theoretical and numerical points of view.

2 Linear elastic fracture mechanics

In this section, we introduce the J-integral concept within the framework of LEFM. As the name implies, in LEFM we are concerned with crack propagation criteria of a pre-cracked elastic body that undergoes small deformations.

2.1 The model problem of linearized elasticity

To begin with, we briefly present the linearized elasticity problem. Therefore, let us first introduce the isotropic elastic body which is given by the closure of a bounded open set $\Omega \subset \mathbb{R}^3$ with a piecewise smooth, polyhedral and Lipschitz continuous boundary Γ such that $\Gamma = \bar{\Gamma}_D \cup \bar{\Gamma}_N$ and $\Gamma_D \cap \Gamma_N = \emptyset$, where Γ_D and Γ_N are the portions of the boundary Γ where Dirichlet and Neumann boundary conditions are imposed, respectively. Assuming, for the sake of simplicity, homogeneous Dirichlet boundary conditions, all admissible displacements $\boldsymbol{u} : \bar{\Omega} \to \mathbb{R}$ of the elastic body $\bar{\Omega}$ are elements of the Hilbert space $\mathcal{V} = \{\boldsymbol{v} \in [H^1(\Omega)]^3 \; ; \; \boldsymbol{v}|_{\Gamma_D} = \boldsymbol{0}\}$.

The weak formulation of the linearized elasticity problem—which is also termed the primal problem throughout this paper—then reads: find $\boldsymbol{u} \in \mathcal{V}$ such that

$$a(\boldsymbol{u}, \boldsymbol{v}) = F(\boldsymbol{v}) \quad \forall \boldsymbol{v} \in \mathcal{V} \tag{1}$$

with the continuous, symmetric and $\mathcal{V}$-elliptic bilinear form $a : \mathcal{V} \times \mathcal{V} \to \mathbb{R}$ and the continuous linear form $F : \mathcal{V} \to \mathbb{R}$ defined by

$$a(\boldsymbol{u}, \boldsymbol{v}) = \int_\Omega \boldsymbol{\sigma}(\boldsymbol{u}) : \boldsymbol{\varepsilon}(\boldsymbol{v}) \; \mathrm{d}V \tag{2}$$

and

$$F(\boldsymbol{v}) = \int_{\Gamma_N} \bar{\boldsymbol{t}} \cdot \boldsymbol{v} \; \mathrm{d}A, \tag{3}$$

respectively. Here, $\boldsymbol{\sigma} = \mathbb{C}_\sigma : \boldsymbol{\varepsilon}$ denotes the stress tensor given in terms of the fourth-order elasticity tensor $\mathbb{C}_\sigma$ and the second-order strain tensor $\boldsymbol{\varepsilon}$ defined as the symmetric gradient of $\boldsymbol{u}$. Furthermore, $\bar{\boldsymbol{t}} \in [L_2(\Gamma_N)]^3$ are prescribed tractions imposed on the Neumann boundary Γ_N. For the sake of simplicity, body forces are omitted in the above formulation.

The discrete counterpart of the variational problem (1) then consists in seeking a solution $\boldsymbol{u}_{1h}$ in a finite-dimensional subspace $\mathcal{V}_{1h} \subseteq \mathcal{V}$ satisfying

$$a(\boldsymbol{u}_{1h}, \boldsymbol{v}_{1h}) = F(\boldsymbol{v}_{1h}) \quad \forall \boldsymbol{v}_{1h} \in \mathcal{V}_{1h}. \tag{4}$$

In order to construct $\mathcal{V}_{1h}$ we first generate a triangulation $\mathcal{T}_{1h}$ of the elastic body $\bar{\Omega}$. Throughout this paper, the finite element associated with each triangle $\bar{\Omega}_{1e} \in \mathcal{T}_{1h}$ is chosen as the well-known simple finite element of the P_1-type.

Subtracting the finite element solution from the true solution, we may define the discretization error as

$$\boldsymbol{e} = \boldsymbol{u} - \boldsymbol{u}_{1h} \in \mathcal{V}. \tag{5}$$

2.2 The J-integral as a crack propagation criterion

In the classical theory of LEFM, three principally different but equivalent scalar-valued crack propagation criteria have been developed in the last century, namely the *energy release rate concept*, the *stress intensity approach*

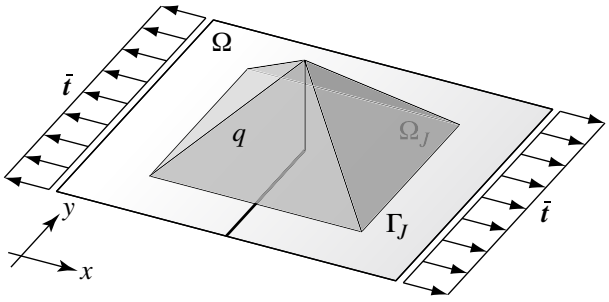

Figure 1: Pre-cracked specimen, boundary conditions and q-function as a pyramid function.

and the *J-integral concept*, as originally proposed by Cherepanov [6] and Rice [15]. For further details on these three concepts the reader may consult the vast literature available, e.g. Anderson [2].

In this paper, we deal with the widely-used J-integral concept. The J-integral, which is a nonlinear functional $J : \mathcal{V} \to \mathbb{R}$, can be conveniently derived by a straightforward application of the concept of material forces, see, e.g., Steinmann et al. [25], since J is the projection of the material force $\boldsymbol{F}_{\text{mat}}$ acting on the crack tip into the direction of crack propagation (given in terms of the unit vector $\boldsymbol{e}_{||}$ which is a priori known in this paper due to symmetry conditions with respect to both the boundary conditions and the geometry of the elastic body), i.e.

$$J(\boldsymbol{u}) = \boldsymbol{F}_{\text{mat}} \cdot \boldsymbol{e}_{||} = \int_{\Gamma_J} \boldsymbol{e}_{||} \cdot \tilde{\boldsymbol{\Sigma}}(\boldsymbol{u}) \cdot \boldsymbol{n} \, \mathrm{d}A \,. \tag{6}$$

Here, Γ_J is an arbitrary contour around the crack tip, $\boldsymbol{n}$ is the unit outward normal to Γ_J and $\tilde{\boldsymbol{\Sigma}}$ denotes the so-called Newton-Eshelby stress tensor given by

$$\tilde{\boldsymbol{\Sigma}} = W_s \boldsymbol{I} - \boldsymbol{H}^T \cdot \boldsymbol{\sigma} \tag{7}$$

with specific strain-energy function W_s, second-order identity tensor $\boldsymbol{I}$ and displacement gradient $\boldsymbol{H}$. Hence, the material force acting on the crack tip can be evaluated in terms of the (material) tractions $\tilde{\boldsymbol{\Sigma}} \cdot \boldsymbol{n}$ at the contour Γ_J. Notice the analogy to a physical force $\boldsymbol{F}_{\text{phy}}$ which can be determined by the (physical) tractions $\boldsymbol{\sigma} \cdot \boldsymbol{n}$.

A pre-existing crack then starts to grow in the direction of $\boldsymbol{e}_{||}$ if J exceeds the (known) material dependent threshold J_c.

From a computational point of view, however, it proves convenient to compute the J-integral by means of the equivalent domain expression

$$J(\boldsymbol{u}) = -\int_{\Omega_J} \boldsymbol{H}(q\boldsymbol{e}_{||}) : \tilde{\boldsymbol{\Sigma}}(\boldsymbol{u}) \, \mathrm{d}V \tag{8}$$

rather than by the contour expression (6). In the above, $q = q(x, y)$ (or $q = q(x, y, z)$ in three space dimensions) represents an arbitrary, piecewise continuously differentiable weighting function with $q = 1$ at the crack tip and

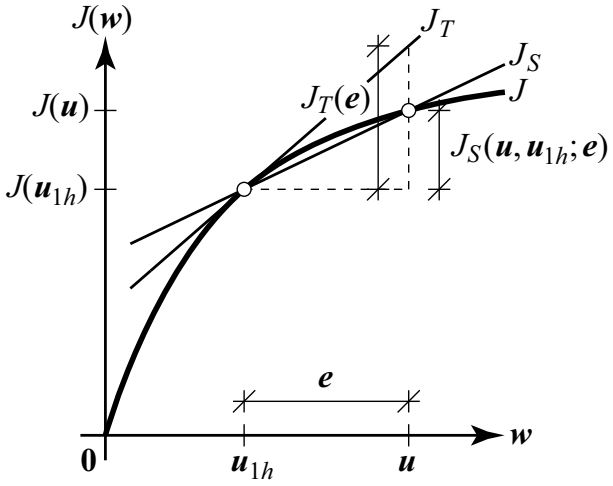

Figure 2: Schematic visualization of the linearizations of the J-integral.

$q = 0$ on the contour (or surface) Γ_J that bounds the area (or volume) Ω_J. For example, q can be conveniently chosen as a pyramid function as shown in Figure 1.

The domain expression (8) was introduced by Shih et al. [22]. For a derivation of (8) in terms of material forces we refer to Heintz et al. [10].

3 The error of the J-integral

3.1 Linearizations of the J-integral

The natural choice for an error measure in linearized elasticity is the energy norm. However, if an engineer is mainly interested in controlling the error of the crack propagation criterion itself, the knowledge of the discretization error measured by the (global) energy norm is not of much use. In this particular case, an engineer is mainly interested in controlling the *goal-oriented* (local) error measure $J(\boldsymbol{u}) - J(\boldsymbol{u}_{1h})$, i.e. the error of the J-integral, within an adaptive mesh refinement scheme. This error measure, however, is nonlinear by definition. Therefore, following the general framework of goal-oriented a posteriori error estimation, see Eriksson et al. [8] and Becker and Rannacher [4], as outlined in Larsson et al. [14] and Rüter et al. [19, 23], we apply the fundamental theorem of calculus on the error measure which yields

$$J(\boldsymbol{u}) - J(\boldsymbol{u}_{1h}) = \int_0^1 J'(\boldsymbol{\xi}(s); \boldsymbol{e}) \, \mathrm{d}s \tag{9}$$

with $\boldsymbol{\xi}(s) = \boldsymbol{u}_{1h} + s\boldsymbol{e}$, $s \in [0, 1]$ and the tangent form of J defined as

$$J'(\boldsymbol{\xi}(s); \boldsymbol{e}) = D_u J(\boldsymbol{u})|_{\boldsymbol{\xi}(s)} \cdot \boldsymbol{e}, \tag{10}$$

that is the Gâteaux derivative of J with respect to $\boldsymbol{u}$ in the direction of $\boldsymbol{e}$. Next, we define a linear functional $J_S : \mathcal{V} \to \mathbb{R}$ by

$$J_S(\boldsymbol{u}, \boldsymbol{u}_{1h}; \boldsymbol{v}) = \int_0^1 J'(\boldsymbol{\xi}(s); \boldsymbol{v}) \, \mathrm{d}s, \tag{11}$$

which represents an exact linearization of the J-integral. Since the exact linearization depends on both the true solution $\boldsymbol{u}$ and its finite element approximation $\boldsymbol{u}_{1h}$, it is a secant form. Combining (11) and (9) with $\boldsymbol{v} = \boldsymbol{e}$, we end up with the important relation

$$J(\boldsymbol{u}) - J(\boldsymbol{u}_{1h}) = J_S(\boldsymbol{u}, \boldsymbol{u}_{1h}; \boldsymbol{e}). \tag{12}$$

It should be emphasized that the above derivation holds for any nonlinear functional J, although in this paper we focus on J defined as the J-integral.

The linearization J_S, however, involves the (generally unknown) exact solution $\boldsymbol{u} \in \mathcal{V}$. Therefore, we shall next introduce a computable approximation J_T of J_S by replacing the exact solution $\boldsymbol{u} \in \mathcal{V}$ with the (known) finite element solution $\boldsymbol{u}_{1h} \in \mathcal{V}_{1h}$. Hence, we arrive at the tangent form

$$J_T(\cdot) = J'(\boldsymbol{u}_{1h}; \cdot) = J_S(\boldsymbol{u}_{1h}, \boldsymbol{u}_{1h}; \cdot) \approx J_S(\boldsymbol{u}, \boldsymbol{u}_{1h}; \cdot) \tag{13}$$

that holds for small errors $\boldsymbol{e}$ only. A schematic visualization of the derivations presented above can be seen in Figure 2.

In this paper, we confine ourselves to the domain expression of the J-integral as defined in (8). In this case, the exact linearization of J reads

$$\begin{aligned} &J_S(\boldsymbol{u}, \boldsymbol{u}_{1h}; \boldsymbol{v}) = \\ &- \int_0^1 \int_{\Omega_J} \boldsymbol{H}(q\boldsymbol{e}_{||}) : \mathbb{C}_\Sigma(\boldsymbol{\xi}(s)) : \boldsymbol{H}(\boldsymbol{v}) \, \mathrm{d}V \, \mathrm{d}s, \end{aligned} \tag{14}$$

whereas the associated tangent form J_T is given by

$$J_T(\boldsymbol{v}) = - \int_{\Omega_J} \boldsymbol{H}(q\boldsymbol{e}_{||}) : \mathbb{C}_\Sigma(\boldsymbol{u}_{1h}) : \boldsymbol{H}(\boldsymbol{v}) \, \mathrm{d}V \, . \tag{15}$$

In the above, $\mathbb{C}_\Sigma$ denotes the fourth-order tensor of elastic tangent moduli associated with the Newton-Eshelby stress tensor defined as

$$\mathbb{C}_\Sigma = \frac{\partial \tilde{\boldsymbol{\Sigma}}}{\partial \boldsymbol{H}} = \boldsymbol{I} \otimes \boldsymbol{\sigma} - \boldsymbol{I} \underline{\otimes} \boldsymbol{\sigma} - \boldsymbol{H}^T \cdot \mathbb{C}_\sigma, \tag{16}$$

see Heintz et al. [10]. Here, "$\underline{\otimes}$" denotes a non-standard dyadic product operator as used e.g. in Steinmann et al. [26]. For further elaborations on the linearizations of the domain as well as the contour expression of the J-integral (6) we refer to Rüter and Stein [21].

3.2 Duality techniques

In order to estimate the error of the J-integral, we follow the general strategy of solving an auxiliary dual problem. The dual problem is based on the dual bilinear form $a^* : \mathcal{V} \times \mathcal{V} \to \mathbb{R}$ defined by $a^*(\boldsymbol{u}, \boldsymbol{v}) = a(\boldsymbol{v}, \boldsymbol{u})$. Since a is symmetric in the case of linearized elasticity, the dual bilinear form a^* coincides with a and the dual problem reads: find a solution $\overset{*}{\boldsymbol{u}} \in \mathcal{V}$ that satisfies

$$a(\overset{*}{\boldsymbol{u}}, \boldsymbol{v}) = J_S(\boldsymbol{u}, \boldsymbol{u}_{1h}; \boldsymbol{v}) \quad \forall \boldsymbol{v} \in \mathcal{V}. \tag{17}$$

As in the case of the primal problem (1), we can, at best, approximate the dual solution $\overset{*}{\boldsymbol{u}}$ by the finite element solution $\overset{*}{\boldsymbol{u}}_{2h} \in \mathcal{V}_{2h} \subseteq \mathcal{V}$ of the uniquely solvable discretized dual problem

$$a(\overset{*}{\boldsymbol{u}}_{2h}, \boldsymbol{v}_{2h}) = J_T(\boldsymbol{v}_{2h}) \quad \forall \boldsymbol{v}_{2h} \in \mathcal{V}_{2h}, \tag{18}$$

where also J_S is approximated by J_T. Here, $\mathcal{V}_{2h}$ is a finite-dimensional subspace of $\mathcal{V}$ constructed on a triangulation $\mathcal{T}_{2h}$ of $\bar{\Omega}$. Following the recent work by Korotov et al. [13, 12] we construct $\mathcal{V}_{2h}$ independently of $\mathcal{V}_{1h}$. Hence, $\mathcal{V}_{2h}$ is generally neither a subspace of $\mathcal{V}_{1h}$ nor is $\mathcal{V}_{1h}$ a subspace of $\mathcal{V}_{2h}$, cf. Rüter et al. [18]. Note that although it is not required that the finite elements associated with each triangle $\bar{\Omega}_{2e} \in \mathcal{T}_{2h}$ are of the same type as used in the primal problem, it clearly proves convenient to use the same finite elements.

Recalling (12) and setting $\boldsymbol{v} = \boldsymbol{e}$ in (17) it is now trivial to observe in the case of small errors $\boldsymbol{e}$ that the error of the J-integral can be exactly represented by

$$J_S(\boldsymbol{u}, \boldsymbol{u}_{1h}; \boldsymbol{e}) = a(\boldsymbol{e}, \overset{*}{\boldsymbol{u}} - \boldsymbol{v}_{2h}) + a(\boldsymbol{e}, \boldsymbol{v}_{2h}), \tag{19}$$

which holds for any $\boldsymbol{v}_{2h} \in \mathcal{V}_{2h}$.

Upon introducing the weak residual of the primal problem $R : \mathcal{V} \to \mathbb{R}$, defined as

$$R(\boldsymbol{v}) = F(\boldsymbol{v}) - a(\boldsymbol{u}_{1h}, \boldsymbol{v}), \tag{20}$$

and setting $\boldsymbol{v}_{2h} = \overset{*}{\boldsymbol{u}}_{2h}$ it is easy to see (by replacing $F(\boldsymbol{v})$ with $a(\boldsymbol{u}, \boldsymbol{v})$ in (20) according to (1)) that (19) can be recast into the following form

$$J_S(\boldsymbol{u}, \boldsymbol{u}_{1h}; \boldsymbol{e}) = R(\boldsymbol{e}_{\overset{*}{u}}) + R(\overset{*}{\boldsymbol{u}}_{2h}), \tag{21}$$

where $\boldsymbol{e}_{\overset{*}{u}} = \overset{*}{\boldsymbol{u}} - \overset{*}{\boldsymbol{u}}_{2h}$ denotes the discretization error of the dual problem.

Likewise, we may further introduce the weak residual of the dual problem $R_{\overset{*}{u}} : \mathcal{V} \to \mathbb{R}$ which is defined as

$$R_{\overset{*}{u}}(\boldsymbol{v}) = J_S(\boldsymbol{u}, \boldsymbol{u}_{1h}; \boldsymbol{v}) - a(\overset{*}{\boldsymbol{u}}_{2h}, \boldsymbol{v}). \tag{22}$$

With this notation at hand, (21) may be equivalently expressed by

$$J_S(\boldsymbol{u}, \boldsymbol{u}_{1h}; \boldsymbol{e}) = R_{\overset{*}{u}}(\boldsymbol{e}) + R(\overset{*}{\boldsymbol{u}}_{2h}), \tag{23}$$

since $R(\boldsymbol{e}_{\overset{*}{u}}) = R_{\overset{*}{u}}(\boldsymbol{e})$, which is, in structural mechanics, also known as Betti's theorem, cf. Cirak and Ramm [7].

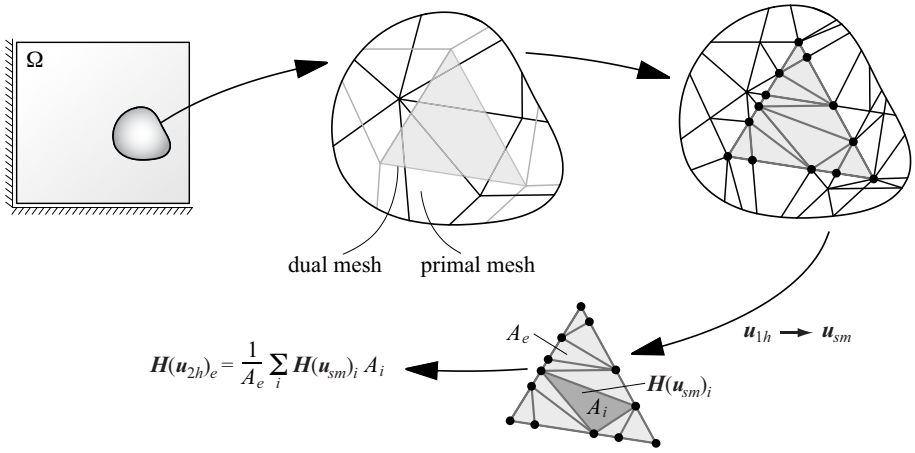

Figure 3: Construction of the supermesh that contains both the primal mesh and the dual mesh.

As a special case, let us construct $\mathcal{V}_{2h}$ such that $\mathcal{V}_{2h} \subseteq \mathcal{V}_{1h}$. In other words, we construct the finite element mesh of the dual problem (18) in such a fashion that it is hierarchically included in the finite element mesh of the primal problem (4). In this case, the dual mesh is generally coarser than the primal mesh. As a limit case, these meshes may also coincide which is the usual strategy to solve the discretized dual problem (18). In these cases, the weak residual $R(\overset{*}{\boldsymbol{u}}_{2h})$ clearly vanishes due to the Galerkin orthogonality. This is easily verified by means of (20) and (4) and the fact that $\overset{*}{\boldsymbol{u}}_{2h} \in \mathcal{V}_{2h} \subset \mathcal{V}_{1h}$. In all other cases the weak residual $R(\overset{*}{\boldsymbol{u}}_{2h})$ is at least exactly computable.

Clearly, the mesh associated with the dual problem does not necessarily have to be coarser than the primal mesh. Also the other case is of special interest where $\mathcal{V}_{1h} \subseteq \mathcal{V}_{2h}$. If we choose quite a fine dual mesh and thus construct $\mathcal{V}_{2h}$ much larger than $\mathcal{V}_{1h}$, then the discretization error $\boldsymbol{e}_u^*$ is quite small compared to $\boldsymbol{e}$. As a consequence, the discrete dual problem (18) needs to be computed only once within the entire adaptive mesh refinement process. This is especially appealing when the dual data is constructed independently of the primal FE-solution $\boldsymbol{u}_{1h} \in \mathcal{V}_{1h}$, which is, however, clearly not the case for the J-integral and other nonlinear functionals, since the linearization always depends on $\boldsymbol{u}_{1h}$.

Summarizing the above, the approach presented can be seen as a generalization of the common strategy to solve the discrete primal and dual problems on the same mesh. As such, the limit case of coinciding meshes for the discrete primal and dual problem is clearly included in this approach as a special case.

3.3 Transfer of the finite element solution

As it turns out in general, for the computation of the approximate dual solution $\overset{*}{\boldsymbol{u}}_{2h} \in \mathcal{V}_{2h}$ a transfer of the primal finite element solution $\boldsymbol{u}_{1h} \in \mathcal{V}_{1h}$ into the finite-dimensional subspace $\mathcal{V}_{2h}$ is required, since J_T depends

explicitly on $\boldsymbol{u}_{1h} \in \mathcal{V}_{1h}$ as was already observed in (15). Clearly, this transfer is trivial whenever $\mathcal{V}_{1h} \subseteq \mathcal{V}_{2h}$. In this paper, however, we construct $\mathcal{V}_{2h}$ in such a fashion that the dual finite element mesh is coarser than the primal mesh. Moreover, in general we have $\mathcal{V}_{2h} \not\subseteq \mathcal{V}_{1h}$.

The transfer of the solution $\boldsymbol{u}_{1h} \in \mathcal{V}_{1h}$ into the finite-dimensional subspace $\mathcal{V}_{2h}$ can be carried out by means of the so-called *supermesh strategy*. A supermesh is a finite element mesh that contains both the mesh associated with the primal and the dual problem.

In order to construct the supermesh, we first create a new partition of the elastic body such that

$$\bar{\Omega} = \bigcup_{i,j} \bar{\Omega}_{1e,i} \cap \bar{\Omega}_{2e,j} \tag{24}$$

with $\bar{\Omega}_{1e,i} \in \mathcal{T}_{1h}$ and $\bar{\Omega}_{2e,j} \in \mathcal{T}_{2h}$. In general, however, this new partition is not a triangulation of $\bar{\Omega}$, since the intersection of (the interiors of) two elements $\Omega_{1e,i} \cap \Omega_{2e,j}$ is either a triangle, a quadrilateral, a pentagon or a hexagon whenever it is non-empty, cf. Figure 3 where three of the four cases are visualized. Hence, if the intersection is non-empty and not a triangle, the non-triangular element is refined until we found a triangulation $\mathcal{T}_{sm}$ of the closed domain $\bar{\Omega}$. This procedure is depicted schematically in Figure 3. As can be observed, degenerated elements may occur in this fashion. In the numerical examples presented in Section 5, it can be seen that such elements have in fact only a small influence on the estimated error.

In practical examples, however, it proves very convenient to make use of the special case where one mesh is hierarchically included in the other. In this fashion, only one initial triangulation of the structure under consideration is required, since the different meshes for the primal and the dual problem result from adaptive mesh refinements. This has the further advantage that the construction of the supermesh is always trivial (since it coincides with the finer mesh) and thus degenerated elements cannot occur. Moreover, in this case it becomes also possible to extend the strategy straightforwardly to three-dimensional problems.

Now it is easily verified that the solution $\boldsymbol{u}_{1h} \in \mathcal{V}_{1h}$ is also an element of the finite-dimensional subspace $\mathcal{V}_{sm} \subseteq \mathcal{V}$ of the supermesh, since $\mathcal{V}_{1h} \subseteq \mathcal{V}_{sm}$. Obviously, the supermesh is constructed such that also $\mathcal{V}_{2h} \subseteq \mathcal{V}_{sm}$ holds. Note that in the special case where one mesh is hierarchically included in the other, we find that either $\mathcal{V}_{sm} = \mathcal{V}_{1h}$ or $\mathcal{V}_{sm} = \mathcal{V}_{2h}$.

Recalling the linearization of the J-integral (15), it is immediately evident that only gradients of the solution $\boldsymbol{u}_{1h} \in \mathcal{V}_{1h}$ have to be transferred into $\mathcal{V}_{2h}$. Since the gradients are constant in each triangle of the supermesh, the transferred gradient is computed as the weighted average of all supermesh elements that are contained in one element of the dual mesh as visualized in Figure 3.

It should finally be noted that the procedure described above does not have to be repeated over all elements of the dual mesh triangulation $\mathcal{T}_{2h}$, since the linearized J-integral J_T is evaluated over the subdomain Ω_J only.

4 Goal-oriented a posteriori error estimation

4.1 The error estimator

Now that we have at our disposal the finite element solutions $\boldsymbol{u}_{1h} \in \mathcal{V}_{1h}$ and $\overset{*}{\boldsymbol{u}}_{2h} \in \mathcal{V}_{2h}$ as well as the error representations for the error of the J-integral (19), (21) and (23) we show next how a posteriori error estimates for the error of the J-integral can be established.

Recalling the error representation (21), the error of the J-integral could be computed if the weak residuals on the right-hand side of (21) were exactly computable. As was already pointed out, the second term, i.e. $R(\overset{*}{\boldsymbol{u}}_{2h})$, is indeed exactly computable. Thus, upper and lower bounds on the error of the J-integral can be derived if the weak residual $R(\boldsymbol{e}^{*}_{u})$ can be bounded from above and from below. For finding such error bounds, various strategies based on residual- hierarchical or averaging-type error estimates have been developed in recent years, see e.g. Ainsworth and Oden [1] and Stein and Rüter [23] for a brief survey.

In this paper, however, we follow the general idea of Zienkiewicz and Zhu [28] and aim at approximating the weak residual $R(\boldsymbol{e}^{*}_{u})$ by an averaging technique in the sense that the approximate gradient fields, that appear in the weak residual, are recovered. In this fashion, upper or lower bounds on the error cannot generally be obtained. However, a sufficiently sharp estimate without bounding properties can be expected. For the derivation of reliable and efficient averaging techniques we refer to Rodríguez [16] and Carstensen and Funken [5].

As was already mentioned, the cornerstone of goal-oriented averaging error estimators is the construction of recovered gradient fields $\boldsymbol{\varepsilon}^{*}(\boldsymbol{u}_{1h})$ and $\boldsymbol{\varepsilon}^{*}(\overset{*}{\boldsymbol{u}}_{2h})$ for both the primal and the dual problem that are "better" approximations of the exact gradient fields $\boldsymbol{\varepsilon}(\boldsymbol{u})$ and $\boldsymbol{\varepsilon}(\overset{*}{\boldsymbol{u}})$ than the ones obtained by the finite element solutions $\boldsymbol{u}_{1h}$ and $\overset{*}{\boldsymbol{u}}_{2h}$, respectively. This qualitative proposition can be turned into the following quantitative statements

$$\|\boldsymbol{\varepsilon}(\boldsymbol{u}) - \boldsymbol{\varepsilon}^{*}(\boldsymbol{u}_{1h})\|_{L_2(\Omega)} \leq C_1 \|\boldsymbol{\varepsilon}(\boldsymbol{u}) - \boldsymbol{\varepsilon}(\boldsymbol{u}_{1h})\|_{L_2(\Omega)} \tag{25}$$

and

$$\|\boldsymbol{\varepsilon}(\overset{*}{\boldsymbol{u}}) - \boldsymbol{\varepsilon}^{*}(\overset{*}{\boldsymbol{u}}_{2h})\|_{L_2(\Omega)} \leq C_2 \|\boldsymbol{\varepsilon}(\overset{*}{\boldsymbol{u}}) - \boldsymbol{\varepsilon}(\overset{*}{\boldsymbol{u}}_{2h})\|_{L_2(\Omega)} \tag{26}$$

with constants $C_1, C_2 \in [0, 1)$.

With the definition of the weak residual (20) and the bilinear form (2) as well as the linear functional (3) we then obtain the goal-oriented a posteriori error estimator

$$J(\boldsymbol{u}) - J(\boldsymbol{u}_{1h}) \approx \sum_{\bar{\Omega}_{1e} \in \mathcal{T}_{1h}} \{\eta_{1e} + \eta_{2e,a} - \eta_{2e,b}\} \tag{27}$$

with element contributions

$$\eta_{1e} = \int_{\Omega_{1e}} [\boldsymbol{\varepsilon}^{*}(\boldsymbol{u}_{1h}) - \boldsymbol{\varepsilon}(\boldsymbol{u}_{1h})] : \mathbb{C}_{\sigma} : \left[\boldsymbol{\varepsilon}^{*}(\overset{*}{\boldsymbol{u}}_{2h}) - \boldsymbol{\varepsilon}(\overset{*}{\boldsymbol{u}}_{2h})\right] \, \mathrm{d}V \tag{28a}$$

as well as

$$\eta_{2e,a} = \int_{\partial\Omega_{1e}\cap\Gamma_N} \bar{\boldsymbol{t}} \cdot \overset{*}{\boldsymbol{u}}_{2h} \, \mathrm{d}A \tag{28b}$$

and

$$\eta_{2e,b} = \int_{\Omega_{1e}} \boldsymbol{\varepsilon}(\boldsymbol{u}_{1h}) : \mathbb{C}_\sigma : \boldsymbol{\varepsilon}(\overset{*}{\boldsymbol{u}}_{2h}) \, \mathrm{d}V \, . \tag{28c}$$

4.2 On the computation of the error estimator

In order to be able to compute the error estimator (27), we first have to determine the recovered gradient fields $\boldsymbol{\varepsilon}^*(\boldsymbol{u}_{1h})$ and $\boldsymbol{\varepsilon}^*(\overset{*}{\boldsymbol{u}}_{2h})$ on the finite element meshes of the primal and the dual problem, respectively. Although all the fields to be recovered are generally discontinuous on the interelement boundaries, a continuous and therefore improved field can be easily created by means of the ansatz functions for the generally C^0-continuous displacement field as used to compute the finite element solutions $\boldsymbol{u}_{1h}$ and $\overset{*}{\boldsymbol{u}}_{2h}$.

As a consequence, appropriate nodal values are required. For this purpose, various strategies have been developed in recent years. Maybe the simplest one, which is used in this paper, is to average the nodal values obtained from the adjacent elements weighted by the area of these elements, see Hlaváček and Křížek [11]. A more advanced strategy is the so-called superconvergent patch recovery technique (SPR technique) as introduced by Zienkiewicz and Zhu [29]. For further details on the SPR technique in the framework of goal-oriented error estimators in nonlinear elastic fracture mechanics we refer to Rüter and Stein [20].

Once these recovered gradient fields are available on both the primal and the dual mesh, the error estimator (27) can be computed by means of the sum of the element contributions from each element $\bar{\Omega}_{1e}$ of the primal mesh. This requires a transformation of the dual solution $\overset{*}{\boldsymbol{u}}_{2h}$ into $\mathcal{V}_{1h}$. In principle, this transformation can be carried out in much the same way as elaborated in Section 3.3. However, a quadrature rule of higher order is required. More precisely, the integrals in (27) are evaluated numerically by the following well-known quadrature formula

$$\int_{\Omega_{1e}} \boldsymbol{\varepsilon}^*(\boldsymbol{u}_{1h}) dV \approx \frac{1}{3} \operatorname{meas} \Omega_{1e} \sum_{i=1}^{3} \boldsymbol{\varepsilon}^*(\boldsymbol{u}_{1h}(\boldsymbol{m}_i)), \tag{29}$$

where $\boldsymbol{m}_i$ are the midpoints of the sides of each triangular element $\bar{\Omega}_{1e} \in \mathcal{T}_{1h}$ of the primal mesh.

Clearly, for the evaluation of (27) we also have to compute the values $\boldsymbol{\varepsilon}^*(\overset{*}{\boldsymbol{u}}_{2h}(\boldsymbol{m}_i))$ for $i = 1, 2, 3$. Generally, however, one has to take into account that the midpoints $\boldsymbol{m}_i$ of the sides of each triangular element $\bar{\Omega}_{1e} \in \mathcal{T}_{1h}$ of the primal mesh are not on the midpoints of the sides of each triangular element $\bar{\Omega}_{2e} \in \mathcal{T}_{2h}$ of the dual mesh as visualized in Figure 4. Thus, the point values $\boldsymbol{\varepsilon}^*(\overset{*}{\boldsymbol{u}}_{2h}(\boldsymbol{m}_i))$ for $i = 1, 2, 3$ have to be carefully determined which is of course trivial in the case of linear triangles.

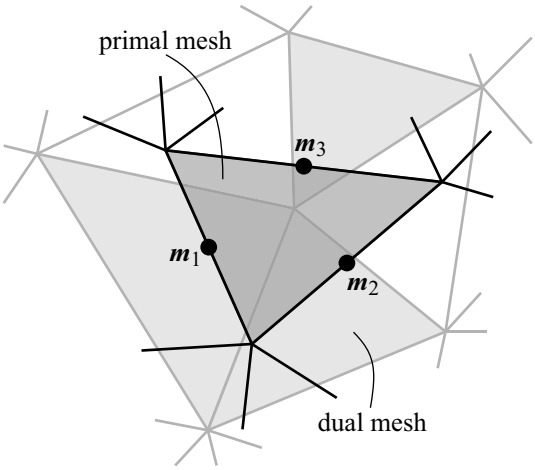

Figure 4: Numerical integration points $\boldsymbol{m}_i$ to compute the error estimator (27) on the primal and the dual mesh.

The computation of the point values $\boldsymbol{\varepsilon}(\boldsymbol{u}_{1h}(\boldsymbol{m}_i))$ and $\boldsymbol{\varepsilon}(\overset{*}{\boldsymbol{u}}_{2h}(\boldsymbol{m}_i))$ for $i = 1, 2, 3$ turns out to be quite easy, since the finite element strain fields are constant in each element.

We further remark that only the error estimator (27) is integrated numerically with the above quadrature rule (29). All other integrals are integrated numerically using one quadrature point in the center of the triangle.

It should finally be noted that the accuracy of the numerical integration scheme as presented above is further improved by subdividing each element of the primal mesh $\bar{\Omega}_{1e}$ uniformly into several subtriangles.

5 Numerical Examples

In this section, we present two numerical examples showing the performance of the goal-oriented a posteriori error estimator (27) based on different meshes for the primal and the dual problem. The required algorithms have been implemented in a Matlab© finite element code that has been developed at the University of Jyväskylä and at Helsinki University of Technology, Finland.

5.1 Plate with a central hole

The system considered in this first numerical example is a pre-cracked glass plate with a central hole in plane-stress state subjected to horizontal tension loads. Due to symmetry considerations only one quarter of the system needs to be modeled. Further information about the geometry of the plate can be gathered from Figure 5. The material data for the plate is assumed as follows: Young's modulus $E = 64000$ N/mm^2, Poisson's ratio $\nu = 0.2$ and critical value $J_c = 0.015$ kJ/m^2 which corresponds to borosilicate glass. The reference value for the given loads was determined using around 100000

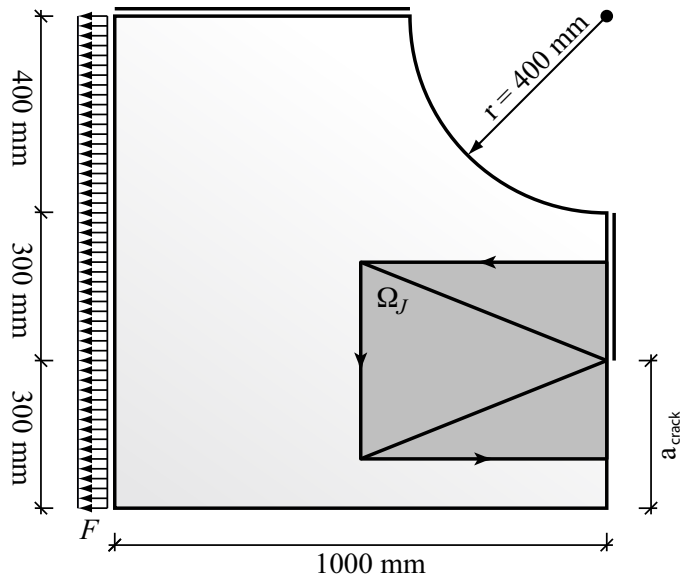

Figure 5: Plate with a central hole, modeled quarter of the system, boundary conditions and integration domain Ω_J for the domain expression of the J-integral which is separated into three parts according to the pyramid function q defined on Ω_J.

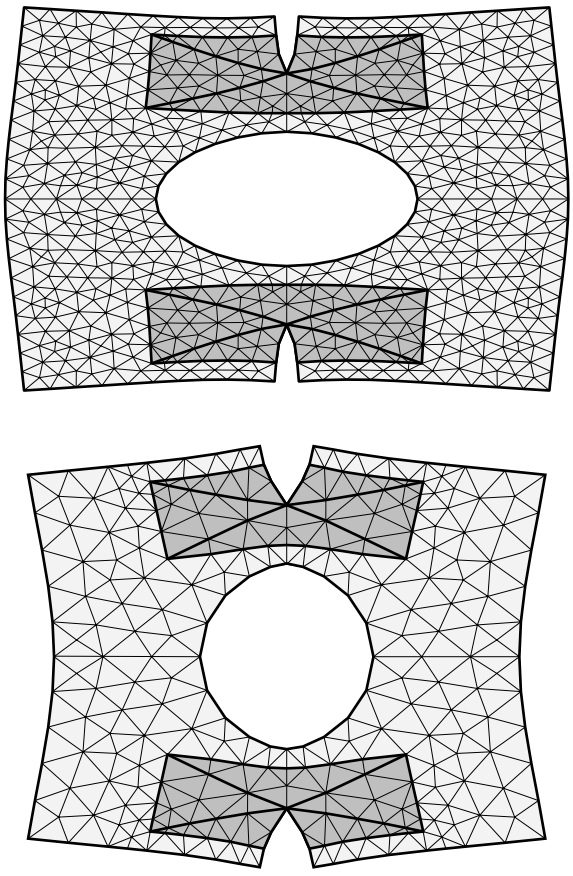

Figure 6: Deformed primal (top) and dual (bottom) meshes.

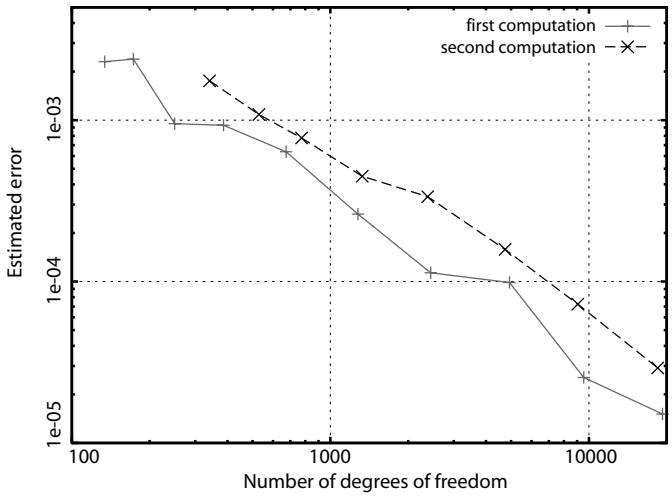

Figure 7: Estimated error measures $J(\boldsymbol{u}) - J(\boldsymbol{u}_{1h})$.

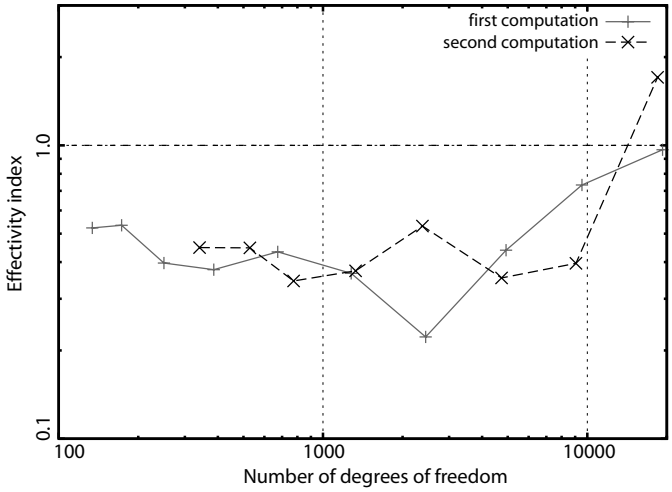

Figure 8: Effectivity indices.

degrees of freedom and reads $J/2 = 0.0129$ kJ/m^2. Thus, under the given loading $F = 0.5$ N/mm^2 the crack will propagate.

Our aim in this example is to investigate how the choice of different dual meshes with different degrees of freedom, that are either hierarchically included in the primal mesh or entirely different from the primal mesh, influence the error estimator. More precisely, in the first computation, both the initial primal and the dual mesh are identical with 134 degrees of freedom. In the second computation, the initial mesh of the primal problem has 341 degrees of freedom whereas the dual mesh is not hierarchically included in the primal mesh and has 131 degrees of freedom.

The associated deformations in the latter case are depicted in Figure 6. Clearly, the deformations are magnified, since both the primal and dual problem are linear.

In both computations investigated, the dual mesh remains the same in each adaptive computation, i.e. only the primal mesh is refined within the

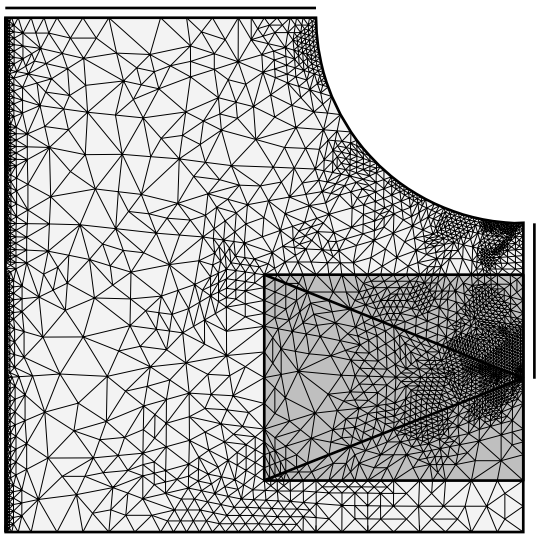

Figure 9: Adaptively refined primal mesh, 19267 degrees of freedom.

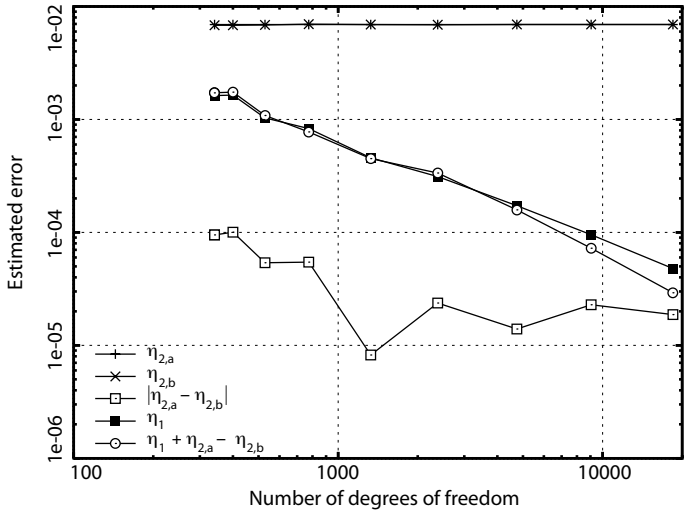

Figure 10: Estimated error splitted into contributions according to (27).

adaptive mesh refinement scheme. Thus, as was already pointed out, the strategy proposed is quite inexpensive compared to the straightforward approach where the dual solution is computed on the same mesh as the primal problem in each adaptive step.

In Figure 7, the estimated error of the J-integral for both computations is plotted. Both estimators investigated show an optimal convergence curve. Apparently, the estimated error in each adaptive refinement step is higher in the case where the dual mesh is not hierarchically included in the primal mesh, which becomes immediately evident, since the initial mesh of the primal problem is much finer compared to the first computation. Therefore, compared to the first computation, the solution of the second computation based on this uniform initial mesh is not as accurate as the solution based on an adaptively refined mesh for the same number of degrees of freedom.

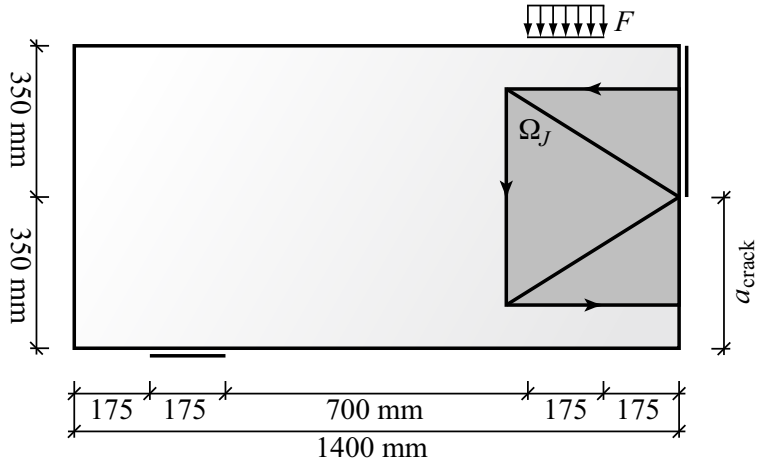

Figure 11: Parallel-edge-cracked plate, modeled system, boundary conditions and integration domain Ω_J for the domain expression of the J-integral which is separated into three parts according to the pyramid function q defined on Ω_J.

The associated effectivity indices, i.e. the ratio of the estimated error to the true error, are visualized in Figure 8 and show that both computations result in a similar effectivity. This, in turn, means that it makes no difference whether or not the dual mesh is hierarchically included in the primal mesh. Moreover, the effectivity indices demonstrate that the approach presented yields quite sharp error estimates that become even sharper with more degrees of freedom.

In this paper, an element is refined if the scaled error indicator at the element level, i.e. the error indicator divided by the largest error indicator, exceeds a given tolerance. The refined primal mesh obtained by this strategy with 19267 degrees of freedom of the last adaptive step is shown in Figure 9. It can be observed that the mesh is heavily refined on the hole and around the crack tip which could clearly be expected because of the stress singularity at the crack tip.

However, the mesh is also refined along the Neumann boundary which can be explained by means of Figure 10 where the (global) error contributions η_1, $\eta_{2,a}$ and $\eta_{2,b}$ according to the definitions in (28) are plotted for the case of our second computation. Clearly, the boundary term $\eta_{2,a}$ remains constant during the adaptive mesh refinement process, since the dual solution is computed on one mesh only. Consequently, $\eta_{2,a}$ gets more and more dominant compared to the estimated term η_1. Furthermore, the volume term $\eta_{2,b}$ is of about the same order than $\eta_{2,a}$. However, the number of elements that share the Neumann boundary Γ_N is much less than the total number of elements. The conclusion to be drawn is that the element contributions $\eta_{2e,a}$ are much higher than $\eta_{2e,b}$ and η_{1e} which results in the heavy mesh refinements observed along the Neumann boundary Γ_N.

Furthermore, Figure 10 shows the interesting result that with increasing number of degrees of freedom the part $\eta_{2,a} - \eta_{2,b}$ contributes more and more

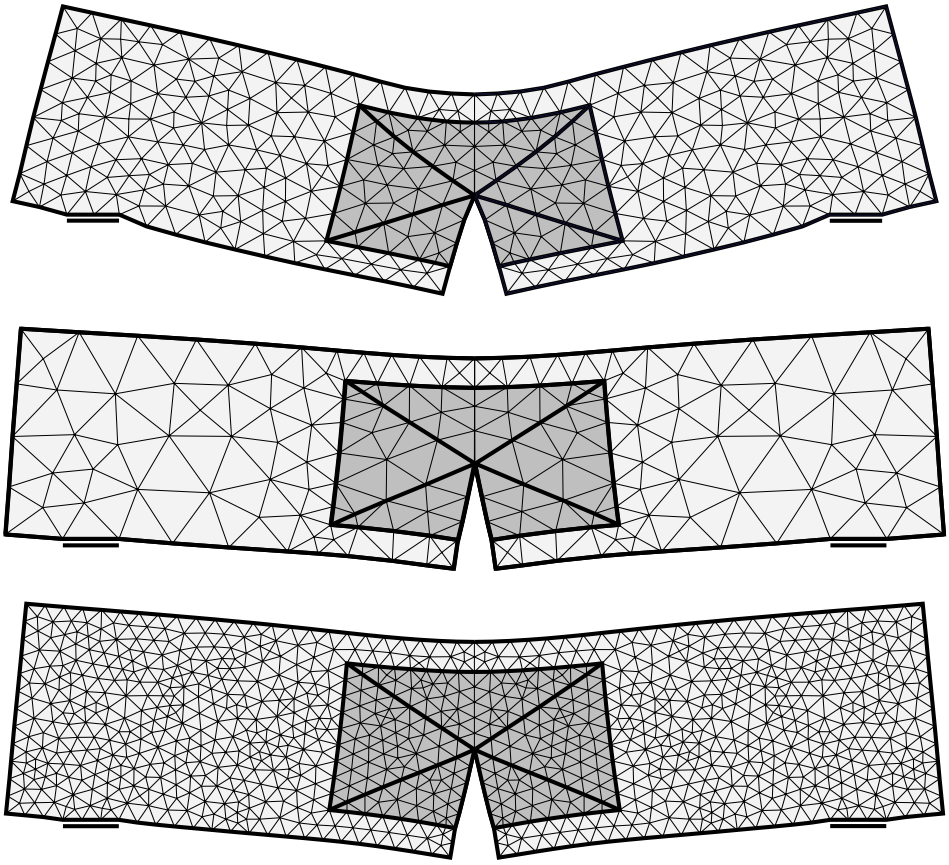

Figure 12: Deformed primal solution (top) as well as deformed dual solutions of the first (middle) and the second (bottom) computation.

to the error estimator (27) compared to η_1. Thus, for rather fine meshes the part η_1 does not have to be computed very accurately in order to get sharp error estimates. In the limit case of extremely fine meshes, η_1 could even be neglected. In this case, the strategy proposed in this paper allows the computation of an error estimator without any term that has to be estimated. As a consequence, this strategy could, in principle, be extended to discretization schemes that are not based on finite elements, e.g. the element free Galerkin method.

5.2 Plate subjected to 4-point bending

In the second numerical example, let us consider a parallel-edge-cracked plate in plane-stress state subjected to 4-point bending, as depicted in Figure 11. The material data is the same as in the previous example, whereas the chosen load in this example is $F = 0.6$ N/mm^2. Due to symmetry considerations, only one half of the specimen is modeled. The reference value for the J-integral is taken from Rüter and Stein [21] and reads $J/2 = 0.012886$ kJ/m^2.

Our objective in this example is to investigate the influence of different dual meshes with different degrees of freedom on the error estimator. To this

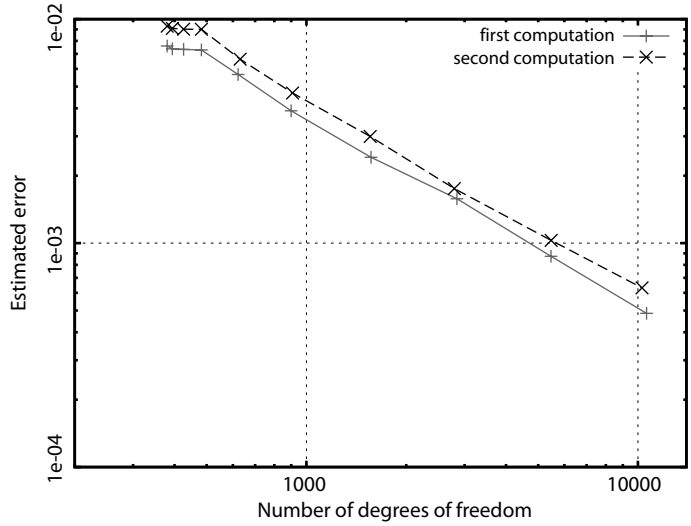

Figure 13: Estimated error measures $J(\boldsymbol{u}) - J(\boldsymbol{u}_{1h})$.

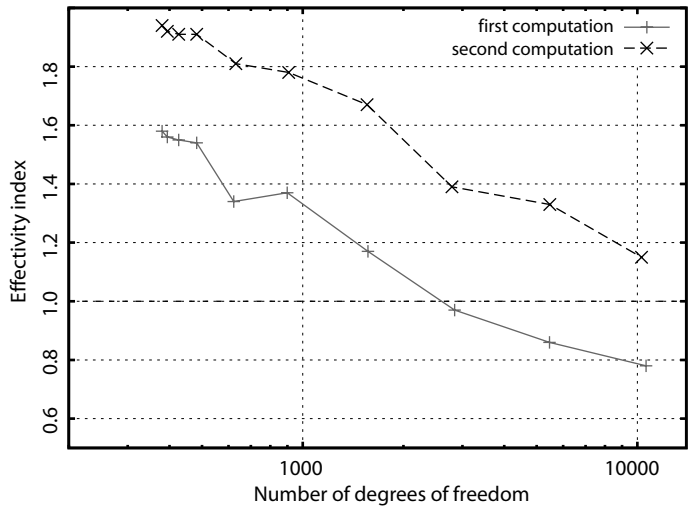

Figure 14: Effectivity indices.

end, again two computations have been carried out. In the first computation, the dual mesh consists of 168 degrees of freedom, whereas in the second computation the dual mesh is constructed such that it has 482 degrees of freedom. In both cases, the dual meshes are not hierarchically related to the primal mesh, which has 380 degrees of freedom in either case. The resulting deformations are depicted in Figure 12.

The associated convergence curves of the estimated error and the corresponding effectivity indices are plotted in Figures 13 and 14, respectively. As in the previous example, the error estimator shows an optimal convergence rate in both cases. At first sight, it seems as if the computation based on the coarser dual mesh yields better results that are closer to the desired value of one. However, the results obtained from the finer dual mesh seem to converge closer to one. Hence, it is obvious that a finer dual mesh yields better

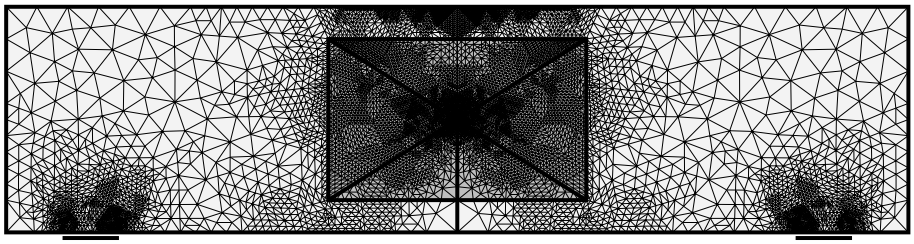

Figure 15: Adaptively refined primal mesh, 11267 degrees of freedom.

results, whereas also the results from the coarser dual mesh are acceptable if one takes into account that the computation is cheaper with a coarser mesh.

Finally, the 9th adaptively refined primal mesh of the first computation can be seen in Figure 15. Again, it can be observed that heavy mesh refinements take place at the singularities, i.e. at the supports and at the crack tip and along the Neumann boundary, especially where we have jumps in the tractions.

6 Conclusions

In this paper, we presented averaging-type goal-oriented a posteriori error estimators for the error of the (nonlinear) J-integral within the framework of linear elastic fracture mechanics. Goal-oriented error estimators are based on the solution of an auxiliary dual problem which was, in this paper, solved on a different mesh than the primal problem. In this fashion, we need to transfer the solutions from one mesh to the other. Furthermore, for the error estimator we obtain an additional term which, in turn, is always exactly computable. On the other hand, the strategy proposed in this paper has the obvious advantage that the dual solution does not have to be computed in every adaptive mesh refinement step and thus reduces the computational costs considerably compared to the common strategy to solve both the primal and the dual problem in each adaptive step on the same mesh. In general, this strategy could be extended to nonlinear model problems such as finite elasticity. However, one has to take into account that in this case, the dual problem depends on the tangent of the last step used in the Newton iterations and therefore leads to certain restrictions. Moreover, in the numerical examples we obtained good numerical evidence for the effectivity of the error estimator presented in this paper.

References

[1] M. Ainsworth and J.T. Oden. *A Posteriori Error Estimation in Finite Element Analysis*. John Wiley & Sons, New York, 2000.

[2] T.L. Anderson. *Fracture Mechanics—Fundamentals and Applications*. CRC Press, Boca Raton, 2. edition, 1995.

[3] I. Babuška and A. Miller. The post-processing approach in the finite element method. Part 3: A posteriori error estimates and adaptive mesh selection. *Int. J. Numer. Meth. Engng*, 20:2311–2324, 1984.

[4] R. Becker and R. Rannacher. A feed-back approach to error control in finite element methods: Basic analysis and examples. *East-West J. Numer. Math.*, 4:237–264, 1996.

[5] C. Carstensen and S.A. Funken. Averaging technique for FE - a posteriori error control in elasticity. Part I: Conforming FEM. *Comput. Methods Appl. Mech. Engrg.*, 190:2483–2498, 2001.

[6] G.P. Cherepanov. Crack propagation in continuous media. *J. Appl. Math. Mech.*, 31:503–512, 1967.

[7] F. Cirak and E. Ramm. A posteriori error estimation and adaptivity for linear elasticity using the reciprocal theorem. *Comput. Methods Appl. Mech. Engrg.*, 156:351–362, 1998.

[8] K. Eriksson, D. Estep, P. Hansbo, and C. Johnson. Introduction to adaptive methods for differential equations. *Acta Numer.*, pages 106–158, 1995.

[9] E. Giner, F.J. Fuenmayor, and J.E. Tarancón. An improvement of the EDI method in linear elastic fracture mechanics by means of an a posteriori error estimator in *G*. *Int. J. Numer. Meth. Engng*, 59:533–558, 2004.

[10] P. Heintz, F. Larsson, P. Hansbo, and K. Runesson. Adaptive strategies and error control for computing material forces in fracture mechanics. *Int. J. Numer. Meth. Engng*, 60:1287–1299, 2004.

[11] I. Hlaváček and M. Křížek. On a superconvergent finite element scheme for elliptic systems. I. Dirichlet boundary condition. *Apl. Mat.*, 32:131–154, 1987.

[12] S. Korotov. Error control in terms of linear functionals based on gradient averaging techniques. *Comp. Lett., in press*, 2005.

[13] S. Korotov, P. Neittaanmäki, and S. Repin. A posteriori error estimation of goal-oriented quantities by the superconvergence patch recovery. *J. Numer. Math.*, 11:33–59, 2003.

[14] F. Larsson, P. Hansbo, and K. Runesson. On the computation of goal-oriented a posteriori error measures in nonlinear elasticity. *Int. J. Numer. Meth. Engng*, 55:879–894, 2002.

[15] J.R. Rice. A path independent integral and the approximate analysis of strain concentration by notches and cracks. *J. Appl. Mech.*, 35:379–386, 1968.

[16] R. Rodríguez. Some remarks on Zienkiewicz-Zhu estimator. *Numer. Methods Partial Differential Equations*, 10:625–635, 1994.

[17] M. Rüter, P. Heintz, F. Larsson, P. Hansbo, K. Runesson, and E. Stein. Strategies for goal-oriented a posteriori error estimation in elastic fracture mechanics. In E. Lund, N. Olhoff, and J. Stegmann, editors, *Proceedings of the 15th Nordic Seminar on Computational Mechanics, NSCM 15, Aalborg, Denmark*, pages 43–46, 2002.

[18] M. Rüter, S. Korotov, and C. Steenbock. A posteriori error estimates in linear elastic fracture mechanics based on different FE-solution spaces for the primal and the dual problem. *Rakenteiden Mekaniikka (Journal of Structural Mechanics)*, 38:87–90, 2005.

[19] M. Rüter, F. Larsson, P. Hansbo, K. Runesson, and E. Stein. Strategies for obtaining goal-oriented a posteriori error estimators in finite elasticity. *Submitted to Comput. & Struct.*, 2004.

[20] M. Rüter and E. Stein. Adaptive finite element analysis of crack propagation in elastic fracture mechanics based on averaging techniques. *Comp. Mat. Sci.*, 31:247–257, 2004.

[21] M. Rüter and E. Stein. Goal-oriented a posteriori error estimates in linear elastic fracture mechanics. *Comput. Methods Appl. Mech. Engrg.*, 195:251–278, 2006.

[22] C.F. Shih, B. Moran, and T. Nakamura. Energy release rate along a three-dimensional crack front in a thermally stressed body. *Intern. J. of Fract.*, 30:79–102, 1986.

[23] E. Stein and M. Rüter. Finite element methods for elasticity with error-controlled discretization and model adaptivity. In E. Stein, R. de Borst, and T.J.R. Hughes, editors, *Encyclopedia of Computational Mechanics*, pages 5–58. John Wiley & Sons, Chichester, 2004.

[24] E. Stein, M. Rüter, and S. Ohnimus. Adaptive finite element analysis and modelling of solids and structures. Findings, problems and trends. *Int. J. Numer. Meth. Engng*, 60:103–138, 2004.

[25] P. Steinmann, D. Ackermann, and F.J. Barth. Application of material forces to hyperelastostatic fracture mechanics. II. Computational setting. *Int. J. Solids Structures*, 38:5509–5526, 2001.

[26] P. Steinmann, R. Larsson, and K. Runesson. On the localization properties of multiplicative hyperelasto-plastic continua with strong discontinuities. *Int. J. Solids Structures*, 34:969–990, 1997.

[27] Z.C. Xuan, N. Parés, and J. Peraire. Computing upper and lower bounds for the J-integral in two-dimensional linear elasticity. *Comput. Methods Appl. Mech. Engrg.*, 195:430–443, 2006.

[28] O.C. Zienkiewicz and J.Z. Zhu. A simple error estimator and adaptive procedure for practical engineering analysis. *Int. J. Numer. Meth. Engng*, 24:337–357, 1987.

[29] O.C. Zienkiewicz and J.Z. Zhu. The superconvergent patch recovery and a posteriori error estimates. Part 1: The recovery technique. *Int. J. Numer. Meth. Engng*, 33:1331–1364, 1992.

(continued from the back cover)

A493 Giovanni Formica , Stefania Fortino , Mikko Lyly
A $vartheta$ method–based numerical simulation of crack growth in linear elastic fracture
February 2006

A492 Beirao da Veiga Lourenco , Jarkko Niiranen , Rolf Stenberg
A posteriori error estimates for the plate bending Morley element
February 2006

A491 Lasse Leskelä
Comparison and Scaling Methods for Performance Analysis of Stochastic Networks
December 2005

A490 Anders Björn , Niko Marola
Moser iteration for (quasi)minimizers on metric spaces
September 2005

A489 Sampsa Pursiainen
A coarse-to-fine strategy for maximum a posteriori estimation in limited-angle computerized tomography
September 2005

A487 Ville Turunen
Differentiability in locally compact metric spaces
May 2005

A486 Hanna Pikkarainen
A Mathematical Model for Electrical Impedance Process Tomography
April 2005

A485 Sampsa Pursiainen
Bayesian approach to detection of anomalies in electrical impedance tomography
April 2005

A484 Visa Latvala , Niko Marola , Mikko Pere
Harnack's inequality for a nonlinear eigenvalue problem on metric spaces
March 2005

HELSINKI UNIVERSITY OF TECHNOLOGY INSTITUTE OF MATHEMATICS
RESEARCH REPORTS

The list of reports is continued inside. Electronical versions of the reports are available at *http://www.math.hut.fi/reports/* .

A498 Marcus Ruter , Sergey Korotov , Christian Steenbock
Goal-oriented Error Estimates based on Different FE-Spaces for the Primal and the Dual Problem with Applications to Fracture Mechanics
March 2006

A497 Outi Elina Maasalo
Gehring Lemma in Metric Spaces
March 2006

A496 Jan Brandts , Sergey Korotov , Michal Krizek
Dissection of the path-simplex in $\mathbf{R}^n$ into n path-subsimplices
March 2006

A495 Sergey Korotov
A posteriori error estimation for linear elliptic problems with mixed boundary conditions
March 2006

A494 Antti Hannukainen , Sergey Korotov
Computational Technologies for Reliable Control of Global and Local Errors for Linear Elliptic Type Boundary Value Problems
February 2006

ISBN 951-22-8129-5
ISSN 0784-3143